Journal of the Chinese Society of Mechanical Engineers, Vol.47, No.3, pp 273~284 (2026)

A Novel Pneumatic Actuator with Linear and Rotary Motion Functions

Yi-Fan Jia*, Zhi-Hao Zhang*, Heng-Yang Zhou*, Chen-Wei Pu*, Yuan-Tong Xu*, Luis Miguel Ruiz Páez*,**and Peng-Fei Qian*

Keywords: Extended state observer; Linear-rotary composite motion; Pneumatic actuator; Sliding mode control;

ABSTRACT

This paper introduces a novel, compact pneumatic actuator capable of executing both rotary and linear motions to enhance work efficiency. Considering the strong nonlinearities inherent in the valve-controlled pneumatic cylinder system and the valve-controlled pneumatic motor system, we employ an extended state observer-based sliding mode control method for the high-precision control of the composite motion pneumatic actuator. The sliding mode control is adopted for its rapid response and good robustness, and the extended state observer is employed to estimate state variables and overall uncertainty of the system in real time. The results indicate that the maximum steady-state error is approximately 0.44 mm when ESO-SMC is used to control the composite motion pneumatic actuator to track a sinusoidal displacement signal with a 0.25 Hz frequency and a 20 mm amplitude. The steady-state error is approximately 2 rpm during the constant rotary speed control of the pneumatic actuator at 800 rpm.

INTRODUCTION

Pneumatic technology (Liu et al., 2019; Ma et al., 2020; Sun et al., 2024) is an engineering technology that employs compressed air as the operational medium and air compressor as the power source for energy and information transfer. This technology is employed in contemporary industrial fields due to its adaptability to complex environments such as flammable, explosive, radiation, and electromagnetic fields.

Paper Received May, 2024. Revised May, 2025. Accept July, 2025. Author for Correspondence: Peng-Fei Qian

* *Department of Mechanical Engineering, Jiangsu University, Zhenjiang, China.*

** *Department of Mechatronic Engineering, Polytechnic University of the Metropolitan Zone of Guadalajara, Tlajomulco de Zúñiga, Mexico.*

Pneumatic cylinders and pneumatic motors are common actuating elements in pneumatic systems. Pneumatic cylinders are used to realize linear reciprocating motion to output force and linear displacement. Pneumatic motors are used to realize continuous rotary motion to output torque and angular displacement. The development of pneumatic actuators has never stopped (Han et al., 2019; Liang et al., 2020; Qian et al., 2023a; Qian et al., 2023b; Saddam et al., 2024; Yue et al., 2022; Zhu et al., 2022). While the pneumatic industry continues to enhance product performance, researchers have also conducted extensive studies and developed novel pneumatic actuators featuring low friction, high efficiency, and high precision. For example, vibration friction reduction pneumatic cylinders (Gao et al., 2016; Pham et al., 2015; Qian et al., 2022a; Qian et al., 2023c), rolling diaphragm-sealed pneumatic cylinders (Whitney et al., 2014), and air-floating frictionless pneumatic cylinders (Qian et al., 2023d) are all novel linear pneumatic cylinders proposed by researchers to enhance pneumatic cylinder performance. In addition, a scroll-type pneumatic motor (Luo et al., 2018) is a representative new type of pneumatic motor proposed in recent years. Through the investigation, it was identified that Festo, a German-based company, has developed a swivel/linear pneumatic cylinder (model DSL-B). This pneumatic cylinder features dual motion modes: a 270° maximum swivel rotation and a 200 mm linear stroke. Crucially, the independent or simultaneous control of these motions provides a unique advantage, driving its widespread industrial adoption. In addition to the continuous enhancement of linear and rotary actuators, there is a growing industrial demand for integrated motion capabilities. Practical applications such as petrochemical explosion-proof valves (Zong et al., 2022), which require both linear thrust and rotary positioning, automated fuel coupling mechanisms (Bi et al., 2021), which involve linear insertion and rotary locking to ensure secure fuel transfer, and fruit-picking end-effectors (Huang et al., 2021; Mao et al., 2022; Xie et al., 2024) that must grip and twist produce, all exemplify scenarios where both linear and rotary motions are indispensable. These examples not only highlight the broad applicability of

pneumatic actuation in delivering explosion-proof, spark-free, and intrinsically safe motion, but also underscore the necessity for compact actuators capable of generating combined motion. Consequently, it is of great research significance to develop a compact end effector that can achieve the combination of rotary and linear motion.

Pneumatic servo control technology has been a persistent focus for researchers in pneumatics (Ahmad et al., 2021; Liao et al., 2022; Qian et al., 2024). The development of early pneumatic servo technology can be traced back to the last century. However, the pneumatic servo system has faced challenges such as low stiffness, low natural frequency, and strong nonlinearity, making it difficult to achieve an ideal control effect using traditional control theories and methods. Consequently, the development of effective control strategies constitutes a central challenge in advancing pneumatic servo control technology. In terms of the position servo control for pneumatic cylinders, Ren et al. successively proposed adaptive backstepping (Ren et al., 2013) and fractional-order proportional-integral-derivative (PID) control (Ren et al., 2019) methods, and found that the latter achieved better control performance compared with the former. Zhao et al. introduced an ESO-based ADRC method to achieve high-precision position control of a rodless pneumatic cylinder (Zhao et al., 2019). The results demonstrate that the controller achieves a very high positioning accuracy with a steady state error within 5 μm, but the trajectory tracking curve shows obvious hysteresis phenomenon. In addition, they proposed a multi-controller positioning strategy (Zhao et al., 2017) and a prescribed performance control strategy based on a nonlinear ESO (Gu et al., 2023) for pneumatic servo systems. Soleymani et al. developed a multiple surface SMC approach, and the results verified the performance of the controller and its good robustness to uncertainties (Soleymani et al., 2017). Qian et al. constructed an integral SMC controller and applied it to a pneumatic motion trajectory tracking system controlled by four switching valves and a pneumatic system based on a vibration friction reduction pneumatic cylinder controlled by a proportional directional valve (Qian et al., 2017; Qian et al., 2022b; Qian et al., 2024b). Meng et al. presented an adaptive robust control (ARC) algorithm to enhance the pneumatic motion tracking accuracy (Meng et al., 2013a; Meng et al., 2013b).

Research on pneumatic motor control remains limited. Safak et al. introduced a trajectory tracking fuzzy logic controller for achieving the speed control of pneumatic motors (Safak et al., 2010). In the experiment, genetic algorithm (GA) was employed to optimize the controller parameters to realize the speed control of the pneumatic motor under different working conditions. Chen et al. designed a PID-based fuzzy neural network controller for the pneumatic motor speed servo system, and proposed an accurate speed control method to address external disturbances and strong nonlinearities within the system (Chen et al., 2016). The results affirm the effectiveness and superiority of this controller. They also proposed an adaptive dynamic SMC method incorporating a PID fuzzy neural network observer (Chen et al., 2017). The results indicate the robustness of the proposed method in addressing the pneumatic motor speed servo system.

The organizational structure of this paper is as follows. Section 2 describes a linear-rotary composite motion pneumatic servo system. The system model is established in Section 3. Section 4 constructs an ESO-SMC controller. Section 5 and Section 6 gives results and discussion, and conclusions and outlook.

PNEUMATIC SERVO SYSTEM BASED ON LINEAR-ROTARY COMPOSITE MOTION PNEUMATIC ACTUATOR

Linear-rotary composite motion pneumatic actuator

To address the limitations in the rotary angle of the DSL-B swivel/linear pneumatic cylinder, this study designs a novel linear-rotary composite motion pneumatic actuator by combining a pneumatic motor and a pneumatic cylinder, as shown in Figure 1. The pneumatic actuator consists of a rotary motion module, a linear motion module and a torque transmission module.

A Gast blade-type pneumatic motor (1AM-NRV-39A) is used as the rotating power source for the rotary motion module. To facilitate the control study of this pneumatic actuator, the information acquisition device for the rotary motion is also considered. In this paper, an Omron rotary encoder is used. As shown in Figure 2(a), the rotary encoder is connected to the rear end cover of the pneumatic motor through an encoder connector and secured with countersunk bolts. In addition, a coupling is used to connect the rotor of the pneumatic motor and the rotating shaft of the rotary encoder, as shown in Figure 2(b). One end of the coupling is provided with a wedge-shaped key to match the rear end of the pneumatic motor, and the other end matches the rotating shaft of the rotary encoder through a set screw to achieve the purpose of measuring the speed of the pneumatic motor.

The linear module utilizes a Festo piston-type pneumatic cylinder (DSBC-32-150-PPVA-N3) to generate linear displacement. The rear end cap of the cylinder is redesigned to facilitate the mechanical integration between the pneumatic cylinder and the pneumatic motor. During installation, the countersunk bolts are screwed into the front cover of the pneumatic motor through the rear cover of the pneumatic cylinder.

To achieve the combination of rotary and linear motions, a torque transmission module is designed, consisting of a sleeve and a transmission rod made of 430F stainless steel. Figure 3 shows the structure of

the through set screws, and the other end is machined to form an "I" shaped hole. One end of the transmission rod fastens to the rodless end of the piston through set screws, and the other end is processed into an "I" shaped shaft, thereby realizing matching transmission with the sleeve. During rotary motion, the torque of the pneumatic motor is transmitted through the torque transmission module to the piston rod of the linear pneumatic cylinder, while overcoming its friction force to drive the piston rod to rotate. During linear motion, relative sliding occurs between the sleeve and the transmission rod, thereby achieving the telescopic movement of the piston rod.

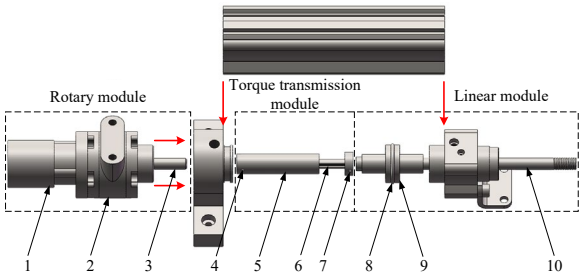

1-Rotary encoder; 2-Pneumatic motor; 3-Rotating shaft; 4, 7-Set screw mounting hole; 5-Sleeve; 6-Transmission rod; 8-Sealing ring; 9-Piston; 10-Piston rod

Fig. 1. Schematic diagram of linear-rotary composite motion pneumatic actuator.

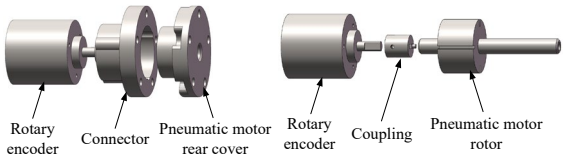

(a) Connector part (b) Coupling part

Fig. 2. Schematic diagram of rotary motion module.

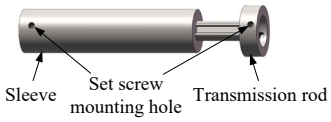

Fig. 3. Schematic diagram of torque transmission module.

Linear-rotary composite motion pneumatic servo system

To investigate the servo control performance of the developed pneumatic actuator, a linear-rotary composite motion pneumatic servo control system is constructed using two Festo proportional valves (MPYE-5-1/8-LF-010-B), as shown in Figure 4. One valve is employed to regulate the air inlet and outlet of the two chambers of the pneumatic cylinder of the linear module. Another one is employed to regulate the air inlet of the inlet chamber of the pneumatic motor of the rotary module, and the pneumatic motor exhaust chamber is exhausted to the atmosphere through a silencer. The pressure values in the pneumatic cylinder chambers and the pneumatic motor inlet chamber are captured using three Huba pressure sensors (511.930002741). The displacement information of the piston is captured in real time by a Panasonic laser displacement sensor (HG-C1200), and the speed information of the pneumatic motor is collected in real time by an Omron rotary encoder (E6B2-CWZ6C). The implementation of control signals for the two proportional valves, along with the acquisition of signals from all sensors, is achieved through a data acquisition card (NI PCI-6221), thereby enabling precise servo control of the linear and rotary motions of linear-rotary composite motion pneumatic actuator.

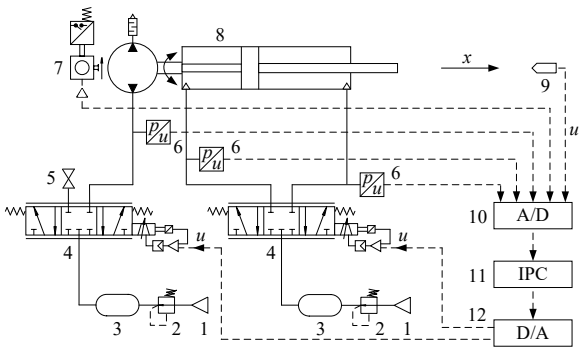

1-Air supply; 2-Pressure reducing valve; 3-Air tank; 4-Proportional directional valve; 5-Stop valve; 6-Pressure sensor; 7-Rotary encoder; 8- Pneumatic actuator; 9-Laser displacement sensor; 10-Digital to analog converter; 11-Industrial computer; 12-Analog to digital converter

Fig. 4. Schematic diagram of linear-rotary composite motion pneumatic servo system.

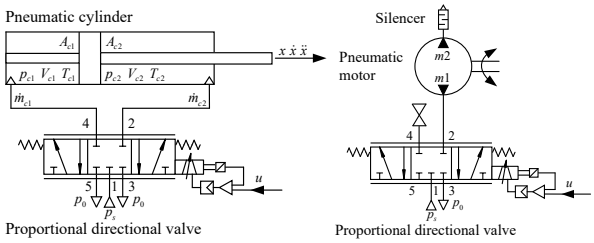

(a) (b)

Fig. 5. (a) Valve-controlled pneumatic cylinder (b) Valve-controlled pneumatic motor.

MATHMATICAL MODELS OF LINEAR -ROTARY COMPOSITE MOTION PNEUMATIC SERVO SYSTEM

The rotary and linear actions of the developed composite motion pneumatic actuator are controlled by two proportional directional valves. Figure 5 shows the schematic diagram of the proportional valve-controlled pneumatic cylinder part and the proportional valve-controlled pneumatic motor part. For the subsequent design of the model-based controller, mathematical models for these two parts are established below.

Models of linear module

Using Newton's second law, the differential equation of the pneumatic cylinder motion can be expressed as

$$M\ddot{x} = A_{c1}p_{c1} - A_{c2}p_{c2} - F_f + f \tag{1}$$

where M is the total mass of the moving parts, $\ddot{x}$ is the acceleration of the piston rod, A_{c1} and A_{c2} are the acted areas of the piston in the transmission rod and piston rod chambers, P_{c1} and P_{c2} are the pressures in the transmission rod and piston rod chambers, F_f is the friction force experienced by the piston-rod assembly as it moves, and f is the uncertainty component of the system.

Due to the compressibility of gas and the variability of thermal processes inside the pneumatic cylinder, the study on cylinder friction is complicated. Therefore, researchers mostly use existing models and identify the model parameters. The combined model of static friction, Coulomb friction and viscous friction is a well-known friction model. However, the discontinuity problem of this model at zero speed causes it to be unsuitable for friction compensation. To this end, the cylinder friction is approximated by the following smooth continuous function (Meng et al., 2013)

$$F_f = A_f S(\dot{x}) + c_v\dot{x} \tag{2}$$

where A_f is the correction coefficient of the smooth friction model, c_v is the viscous friction coefficient, and $S(\dot{x})$ is the Stribeck approximate continuous smooth curve, and it can be chosen as

$$S(\dot{x}) = \frac{2}{\pi}\arctan(1000\dot{x}) \tag{3}$$

Here, to determine the parameters A_f and c_v, the high-precision friction test platform (Qian et al., 2022c) we built previously is utilized to test the steady-state friction of this pneumatic actuator. The test schematic diagram and the measurement results are shown in Figure 6. A ball screw sliding table drives the piston rod at a constant speed, while a force sensor captures the friction force data of the actuator. By fitting the friction test results with the above simplified model, A_f and c_v are obtained to be 2.95 N and 88.81 N·s/m, respectively.

The thermodynamic equation inside the linear pneumatic cylinder is established according to the first law of thermodynamics and the ideal gas law. For the convenience of modeling, it is assumed that no heat exchange occurs between the gas in the chambers and the external atmosphere, i.e., the gas temperature in the chambers is equal to the ambient temperature. Then, thermodynamics can be described as follows

$$\begin{cases} \dot{p}_{c1} = \dfrac{\gamma RT_{c1}}{V_{c1}}(\dot{m}_{c1,in} - \dot{m}_{c1,out}) - \dfrac{\gamma p_{c1}\dot{V}_{c1}}{V_{c1}} \\ \dot{p}_{c2} = \dfrac{\gamma RT_{c2}}{V_{c2}}(\dot{m}_{c2,in} - \dot{m}_{c2,out}) - \dfrac{\gamma p_{c2}\dot{V}_{c2}}{V_{c2}} \\ T_{c1} = T_{c2} = T_0 \end{cases} \tag{4}$$

where R is the ideal gas constant, γ is the gas specific heat ratio, $\dot{m}_{c1,out}$ and $\dot{m}_{c2,out}$ are the inflow mass flow rates corresponding to the transmission rod and piston rod chambers, V_{c1} and V_{c2} are the outflow mass flow rates corresponding to the transmission rod and piston rod chambers, V_{c1} and V_{c2} are the volumes of the transmission rod and piston rod chambers, T_{c1}, T_{c2} and T_0 are temperature of the transmission rod chamber, piston rod chamber, and atmosphere, respectively. V_{c1} and V_{c2} can be expressed as

$$\begin{cases} V_{c1} = V_{1d} + A_{c1}\left(\dfrac{L}{2} + x\right) \\ V_{c2} = V_{2d} + A_{c2}\left(\dfrac{L}{2} - x\right) \end{cases} \tag{5}$$

where V_{1d} and V_{2d} are the dead volumes of the transmission rod and piston rod chambers, and L is the cylinder stroke. Note that x is positive during pneumatic cylinder extending movement, and the cylinder middle position is the zero point.

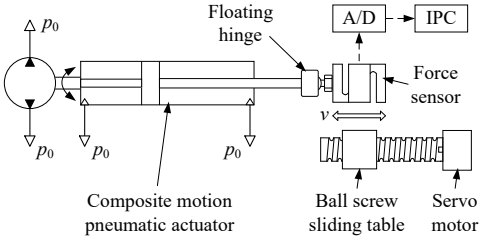

(a) Schematic diagram of friction test

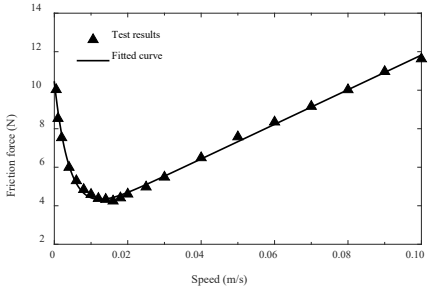

(b) Results of friction test

Fig. 6. Friction test of composite motion pneumatic actuator.

Models of rotary module

As shown in Figure 5(b), it is assumed that compressed air flows into the pneumatic motor chamber from port $m1$ and flows out from port $m2$. During the rotation of the pneumatic motor rotor, the working length x_m of the blade can be described as

$$x_m = d_m \cos\theta_m + \sqrt{R_m{}^2 - d_m{}^2 \sin^2\theta_m} \tag{6}$$

where R_m is the radius of the inner wall of the motor housing, d_m is the eccentricity, and $d_m = R_m - r_m$, in which r_m is the radius of the pneumatic motor rotor, θ_m is the rotary angle of the pneumatic motor.

The torque balance equation for the composite motion pneumatic actuator is described as

$$M_m - M_f = J_m \ddot{\theta}_m \tag{7}$$

where M_m is the driving torque of the pneumatic motor, M_f is the total friction torque of the composite motion pneumatic actuator, J_m is the moment of inertia, and $\ddot{\theta}$ is the angular acceleration of the pneumatic motor.

The torque M_m is determined by the combined torque of the gas in the inlet and outlet chambers acting on the working blade. Assuming that $d_m{}^2\sin^2\theta_m << R_m{}^2$, and then M_m can be expressed as

$$M_m = \frac{1}{2} L_m (p_{m1} - p_{m2})(x_m - r_m)(x_m + r_m) \tag{8}$$

$$= \frac{1}{2} L_m (p_{m1} - p_{m2})(d_m{}^2 \cos 2\theta_m + 2 d_m R_m \cos\theta_m + R_m{}^2 - r_m{}^2)$$

where L_m is the length of the pneumatic motor blade, p_{m1} and p_{m2} are the pressures in the inlet and outlet chambers of the pneumatic motor respectively.

For this composite motion pneumatic actuator, the total friction torque is characterized using a combined model of coulomb and viscous friction. It can be described as

$$M_f = M_c f(\dot{\theta}) + M_v \dot{\theta} \tag{9}$$

where M_c is the coulomb friction torque, and M_v is the viscous friction torque coefficients. $f(\dot{\theta})$ can be expressed as

$$f(\dot{\theta}) = \begin{cases} 0, & \dot{\theta} = 0 \\ \text{sign}(\dot{\theta}), & \dot{\theta} \neq 0 \end{cases} \tag{10}$$

When the pneumatic motor is stationary or rotating at a constant speed, $\ddot{\theta} = 0$, then the total friction torque is equal to its driving torque. Therefore, this study measures the two chamber pressures of the pneumatic motor at different constant speeds to calculate its friction torque, and further identifies the parameters M_c and M_v. As shown in Figure 7(a), the proportional directional valve, the pneumatic motor, and the rotary encoder form a closed-loop speed control system, which can control the pneumatic motor to perform constant rotary speed motion. In addition, two pressure sensors are used to measure the pressure in both chambers of the pneumatic motor. Based on the test results presented in Figure 7(b), we obtain M_c and M_v as 0.1281 N·m and 8.66×10^{-5} N·m/(r/min), respectively.

Models of proportional directional valve

In this study, two FESTO proportional directional control valves were employed. Their flow characteristics were characterized in accordance with the flow equations specified by the international standard ISO 6358, as follows:

$$\dot{m} = \begin{cases} A(u) C_d C_1 \dfrac{p_u}{\sqrt{T_u}}, & \dfrac{p_d}{p_u} \le b \\ A(u) C_d C_1 \dfrac{p_u}{\sqrt{T_u}} \sqrt{1 - \left(\dfrac{\frac{p_d}{p_u} - b}{1 - b} \right)^2}, & \dfrac{p_d}{p_u} > b \end{cases} \tag{11}$$

where $\dot{m}$ is the gas mass flow rate through the valve port, $A(u)$ is the valve opening area, C_1 is a constant, p_u and p_d are the pressures downstream and upstream of the valve port, T_u is the temperature upstream of the valve port, b is the critical pressure ratio, C_d is the correction coefficient, which can be expressed as

$$C_d = 0.8153 + 0.0933 \left(\frac{p_d}{p_u} \right) - 0.1038 \left(\frac{p_d}{p_u} \right)^2 \tag{12}$$

The relationship between the valve opening area $A(u)$ and the control voltage u can be obtained through the flow test of the proportional directional valve, as shown in Figure 8.

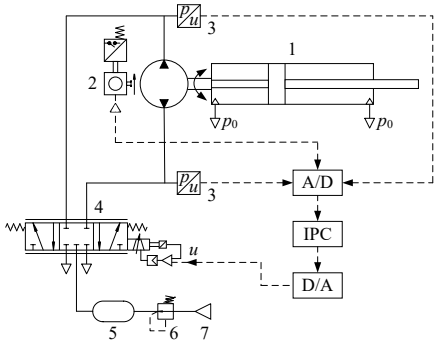

1-Composite motion pneumatic actuator; 2-Rotary encoder; 3-Pressure sensor; 4-Proportional directional valve; 5-Air tank; 6-Pressure reducing valve; 7-Air supply

(a) Schematic diagram of friction torque test

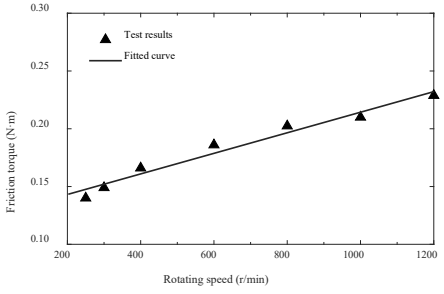

(b) Results of friction torque test

Fig. 7. Friction torque test results of composite motion pneumatic actuator.

CONTROLLER DESIGN

In this study, a sliding mode control (SMC) method is adopted for the rotary and linear motion actuation systems of the composite motion pneumatic actuator due to its fast response and strong robustness. Given the complexity of friction characteristics in the actuator, which arises from the involvement of both linear and rotary motion, an extended state observer (ESO) is further implemented to estimate the state variables and total uncertainty of the system in real time. The ESO helps mitigate the impact of complex frictional behaviors and external disturbances on the system's performance. The schematic diagram of the extended state observer-based sliding mode controller (ESO-SMC) is shown in Figure 9.

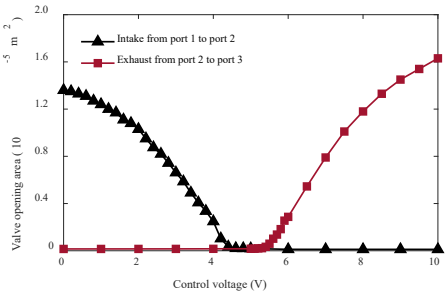

Fig. 8. Relationship between valve opening area and control voltage

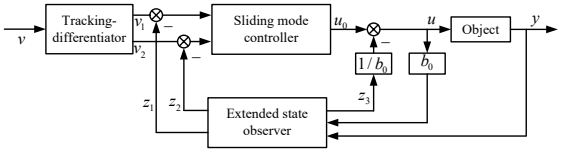

Fig. 9. The schematic diagram of the extended state observer-based sliding mode controller.

Extended state observer

For second-order system $\ddot{y} = f(y, \dot{y}, \omega, t) + b_0 u$ (u is the system input, y is the system output, ω is the disturbance part; b_0 is the known part of the system), it can be expressed in differential form as follows

$$\begin{cases} \dot{x}_1 = x_2 \\ \dot{x}_2 = x_3 + b_0 u \\ \dot{x}_3 = \omega(t) \end{cases} \tag{13}$$

where $y = x_1$, $\dot{y} = x_2$, $f = x_3$, and $\dot{f} = \omega(t)$. The state equation corresponding to the above equation can be expressed as

$$\begin{cases} \dot{x} = Ax + Bu + E\omega(t) \\ y = Cx \end{cases} \tag{14}$$

where $A = \begin{bmatrix} 0 & 1 & 0 \\ 0 & 0 & 1 \\ 0 & 0 & 0 \end{bmatrix}$, $B = \begin{bmatrix} 0 \\ b_0 \\ 0 \end{bmatrix}$, $E = \begin{bmatrix} 0 \\ 0 \\ 1 \end{bmatrix}$, and $C = \begin{bmatrix} 1 & 0 & 0 \end{bmatrix}$.

Then, the corresponding continuous linear extended state observer is as follows

$$\begin{cases} \dot{z} = Az + Bu + L(y - \hat{y}) \\ \hat{y} = Cz \end{cases} \tag{15}$$

where z is the state vector, and L is the error feedback gain matrix.

Although ω is unknown, its value can be estimated through the correction term, so the parameter ω is omitted in Eq. (15). Therefore, the observer equation can be re-expressed as

$$\begin{cases} \dot{z} = [A - LC]z + [B, L]u_c \\ y_c = Cz \end{cases} \tag{16}$$

where $u_c = [u\ y]^T$ is the combined input, and y_c is the output. Let the observer gain matrix L be

$$L = \begin{bmatrix} \beta_1 & \beta_2 & \beta_3 \end{bmatrix}^{\mathrm{T}} = \begin{bmatrix} 3\omega_0 & 3\omega_0^2 & \omega_0^3 \end{bmatrix}^{\mathrm{T}} \tag{17}$$

Therefore, the differential equation of the state observer can be obtained as follows

$$\begin{cases} \dot{z}_1 = z_2 - \beta_1(z_1 - y) \\ \dot{z}_2 = z_3 + b_0 u - \beta_2(z_1 - y) \\ \dot{z}_3 = -\beta_3(z_1 - y) \end{cases} \tag{18}$$

where: z_1, z_2, and $z_3$are the online parameter estimates corresponding to y, $\dot{y}$, and f, respectively, and β_1, β_2, and β_3 are the observer gains. The gains of the observers should satisfy the following condition.

$$\begin{cases} \beta_1 > 0 \\ \beta_2\beta_3 > \beta_3 > 0 \end{cases} \tag{19}$$

It is assumed that the rate of change of the total system disturbance f is bounded, with $\dot{f} < \omega$, $|\omega| < \omega_b$, ω_b is a positive real number.

Define $\hat{e} = z_1 - y$, $\dot{\hat{e}} = z_2 - \dot{y}$ and $\hat{f} = z_3 - f$ as the online estimation errors. By subtracting Eq. (18) from (13), we obtain:

$$\dot{G} = \hat{A}G - E\omega \tag{20}$$

where $G = \begin{bmatrix} \hat{e} \\ \dot{\hat{e}} \\ \hat{f} \end{bmatrix}$, $\hat{A} = \begin{bmatrix} -\beta_1 & 1 & 0 \\ -\beta_2 & 0 & 1 \\ -\beta_3 & 0 & 0 \end{bmatrix}$, $E = \begin{bmatrix} 0 \\ 0 \\ 1 \end{bmatrix}$.

When the observer gains satisfy Eq. (19), the matrix $\hat{A}$ can be concluded as a Hurwitz matrix by the Routh criterion. Therefore, for any positive definite matrix Q, there exists a positive definite symmetric

matrix P such that $\hat{A}^T P + P\hat{A}^T = -Q$.

The defined Lyapunov function can be expressed as follows:

$$V = E^T PE \tag{21}$$

Taking the derivative of the Lyapunov function, we get

$$\begin{aligned} \dot{V} &= \dot{E}^T PE + E^T P\dot{E} \\ &= E^T(\hat{A}^T P + P\hat{A}) - 2\omega E^T PE \\ &= -E^T QE - 2\omega E^T PE \\ &\le -\lambda_{\min}(Q)\|E\|^2 + 2|\omega|\|E\|\|P\|\|E\| \\ &\le -\lambda_{\min}(Q)\|E\|^2 + 2\omega_b\lambda_{\max}(P)\|E\| \end{aligned} \tag{22}$$

where $\lambda_{\min}(Q)$ is the minimum eigenvalue of matrix Q, and $\lambda_{\max}(P)$ is the maximum eigenvalue of matrix P.

Consequently, $||E||$ converges to the set $\Phi = \{E\|\|E\| < 2\omega_b\lambda_{\max}(P)/\lambda_{\min}(Q)\}$, indicating that the observer error is uniformly bounded.

Tracking-differentiator

When ESO is used to reduce the noise in the feedback input signal, a large phase lag is generated, which reduces the stability of the control system. The use of tracking-differentiator (TD) can well alleviate the phase lag phenomenon caused by ESO. A discrete form TD is adopted, as follows

$$\begin{cases} v_1(k+1) = v_1(k) + Tv_2(k) \\ v_2(k+1) = v_2(k) + Tfst[v_1(k), v_2(k), x_{ref}(k), r, h] \end{cases} \tag{23}$$

where h is the filtering factor, r is the speed factor, T is the tracking step, $x_{ref}(k)$ is the input signal, $v_1(k)$ is the tracking output, and $v_2(k)$ is the differential output.

$$\begin{cases} d = rh \\ d_0 = dh \\ y = v_1 - u + hv_2 \\ a_0 = \sqrt{d^2 + 8r|y|} \\ a = \begin{cases} v_2 + y/h, & |y| \le d_0 \\ v_2 + 0.5(a_0 - d)\mathrm{sgn}(y), & |y| > d_0 \end{cases} \\ fst = \begin{cases} -ra/d, & |a| \le d \\ -r\,\mathrm{sgn}(a), & |a| > d \end{cases} \end{cases} \tag{24}$$

The larger the speed factor r is, the faster the system tracks the signal. However, when the internal and external noise of the system is large, the larger the speed factor r will make the tracking signal v_1 more susceptible to the influence of noise. A better filtering effect can be achieved by choosing a suitable filtering factor h. The smaller the filtering factor h, the smaller the phase deviation of the tracking signal v_1 will be.

Sliding mode controller

This section constructs the SMC (ESO-SMC) controller based on ESO for rotary motion and linear motion control of the composite motion pneumatic actuator. The second-order nonlinear affine model of the pneumatic servo system in the rotational motion and linear motion mode is established below.

$$\begin{cases} \dot{x}_1 = x_2 \\ \dot{x}_2 = f_d + f(x) + b_0 u \end{cases} \tag{25}$$

where $f(x) = \dfrac{\gamma A_{c2} p_{c2} V_{c2}}{MV_{c2}} - \dfrac{\gamma A_{c1} p_{c1} V_{c1}}{MV_{c1}} - F_f$.

In this study, a sliding mode surface is selected as follows

$$s = c_1 e + c_2 \int_0^t e\mathrm{d}t + \dot{e} \tag{26}$$

where $e = v_1 - z_1$, $\dot{e} = v_2 - z_2$, $c_1 = {\lambda_R}^2$, $c_2 = 2\lambda_R$.

Taking the derivative of the sliding mode surface s, we get

$$\begin{aligned} \dot{s} &= c_1\dot{e} + c_2 e + \ddot{e} \\ &= c_1\dot{e} + c_2 e + (b_0 u + f(x) + f_{cd} - \ddot{x}_{cr}) \end{aligned} \tag{27}$$

where f_{cd} is the uncertain disturbances ($f_{cd} = z_3$) in the system, and x_{cr} is the reference signal.

Although SMC has the advantages of simple implementation and strong robustness, the dynamic characteristics of the system and the high-frequency oscillation caused by non-ideal switching characteristics are often ignored in its design, which will lead to the chattering phenomenon during the control process.

Therefore, the reaching law method is used in this paper, as follows

$$\dot{s} = -\varepsilon \mathrm{sat}(s) \tag{28}$$

where sat(s) is the saturation function and can be expressed as follows

$$\mathrm{sat}(s) = \begin{cases} 1, & s > \Delta \\ ks, & |s| \le \Delta \\ -1, & s < -\Delta \end{cases} \tag{29}$$

Substituting Eq. (28) into Eq. (27), the ESO-SMC control law for the valve-controlled pneumatic cylinder system is obtained, as follows

$$u = \frac{-\varepsilon \mathrm{sat}(s) + \ddot{x}_{cr} - c_1 e - c_2\dot{e} - f_{cd} - f(x)}{b_0} \tag{30}$$

For the valve-controlled pneumatic motor system, an ESO-SMC controller with friction torque compensation is designed, and its control law is as follows

$$u = \frac{-\varepsilon \mathrm{sat}(s) + \ddot{x}_{mr} - c_1 e - c_2 \dot{e} - f_{md} - M_f}{b_0} \tag{31}$$

where f_{md} is the uncertain disturbances, and x_{mr} is the pneumatic motor control reference signal.

The defined Lyapunov function can be expressed as follows

$$V = \frac{1}{2} s^2 \tag{32}$$

Taking the derivative of the Lyapunov function, we get

$$\begin{aligned} \dot{V} &= s\dot{s} = s(\ddot{e} + c_1 e + c_2 \dot{e}) \\ &= s(\ddot{x} - \ddot{x}_{ref} + c_1 e + c_2 \dot{e}) \\ &= s(f(x) + b_0 u + f_{c,d} - \ddot{x}_{ref} + c_1 e + c_2 \dot{e}) \\ &= s\dot{s} = s(-\varepsilon sat(s)) \le -\varepsilon |s| \end{aligned} \tag{33}$$

It is known through the Lyapunov stability theory that the choice of appropriate parameters can ensure that when $\varepsilon > 0$, the system state will be stabilized at the sliding surface $s = 0$. Eq. (26) can be expressed as follows by Laplace transformation:

$$s^2 E(s) + c_2 s E(s) + c_1 E(s) = 0 \tag{34}$$

The above equation can be viewed as a closed-loop system with e as the output. where the transfer function can be expressed as:

$$G_k(s) = \frac{1}{\lambda_R{}^2}(s^2 + 2\lambda_R s) \tag{35}$$

The phase of this transfer function is greater than -π/2, and there are no poles in the right half-plane. Therefore, according to the Nyquist theorem, it can be inferred that this system is stable. The formula obtained from the Final Value Theorem follows:

$$\lim_{t\to\infty} e = \lim_{t\to\infty} \frac{s}{\lambda_R{}^2}(s^2 + 2\lambda_R s) = 0 \tag{36}$$

It can be known from the above equation that when s tends to zero, the tracking error also tends to zero. Therefore, the output of this pneumatic servo system can track the reference signal.

RESULTS AND DISCUSSION

Experimental setup

Based on the schematic diagram of the linear-rotary composite motion pneumatic servo system, this study establishes a MATLAB/Simulink RTW-based experimental platform for servo control, as illustrated in Figure 10. For motion control experiments of the novel pneumatic actuator, the system operates with a 1 ms sampling period. The supply pressures for the valve-controlled linear module and rotary motion module are set to 0.2 MPa and 0.4 MPa, respectively. The system model parameters are listed in Table 1. Additionally, this paper selects two conventional pneumatic system controllers along with the proposed controller for experimental studies on actuator motion control.

Experimental results

Three controllers are used to control the linear-rotary composite motion pneumatic actuator to track a sinusoidal displacement reference curve with a 0.25 Hz frequency and a 20 mm amplitude, and to perform constant rotary speed control at 800 rpm. In order to compare the motion control experimental results of different controllers, this paper selects two performance evaluation indicators to analyze the motion control experimental results of the controllers.

1) $e_{\max} = \max_{t \ge Ts}\{|e|\}$, the maximum steady-state absolute value of the tracking error, where T_s is the time to reach steady state;

2) RMSE is steady-state root mean square error, where $N = N_2 - N_1$, which can be expressed as follows

$$\mathrm{RMSE} = \sqrt{\frac{1}{N}\sum_{N_1}^{N_2} e_k^2} \tag{37}$$

Table 1. Model parameters of linear-rotary composite motion pneumatic servo system.

Symbol	Value	Unit
A_{c1}	8.04×10^{-4}	m^2
V_{1d}	1.1×10^{-5}	m^3
A_{c2}	6.912×10^{-4}	m^2
V_{2d}	0.6×10^{-5}	m^3
M	0.28	Kg
A_f	2.95	N
c_v	88.81	N·s/m
L	0.15	m
M_c	0.1281	N·m
Mv	8.66×10^{-5}	N·m/(r/min)
b	0.29	-
γ	1.4	-
c_1	0.0404	-
R	287	N·m/(Kg·K)
T_0	300	K

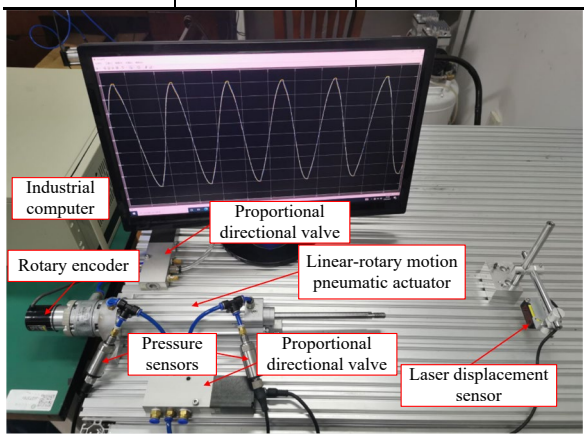

Fig. 10. Experimental platform of linear-rotary composite motion pneumatic servo system.

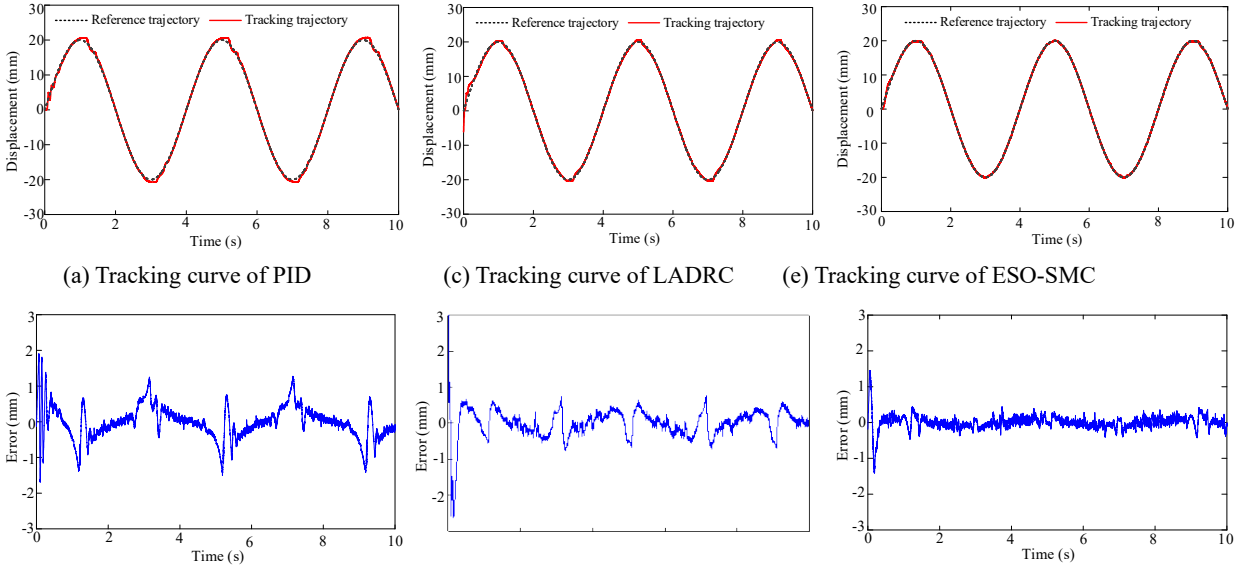

(a) Tracking curve of PID (c) Tracking curve of LADRC (e) Tracking curve of ESO-SMC

(b) Error curve of PID (d) Error curve of LADRC (f) Error curve of ESO-SMC

Fig. 11. Trajectory tracking results for 0.25 Hz sinusoidal displacement reference curve.

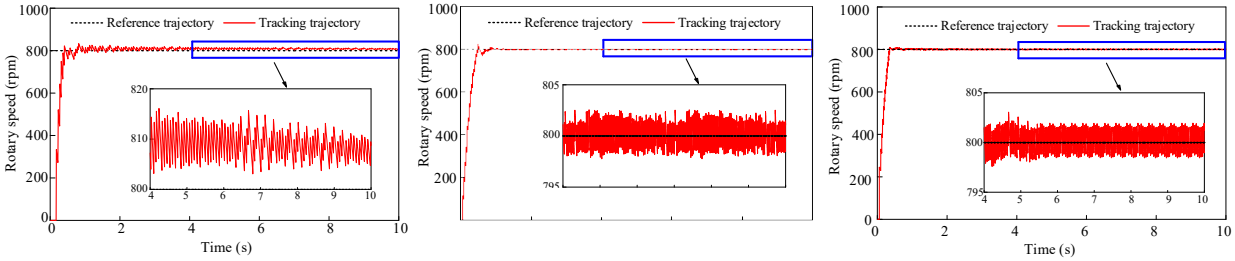

(a) Tracking curve of PID (b) Tracking curve of LADRC (c) Tracking curve of ESO-SMC

Fig. 12. Trajectory tracking results for 800 rpm rotary speed reference curve.

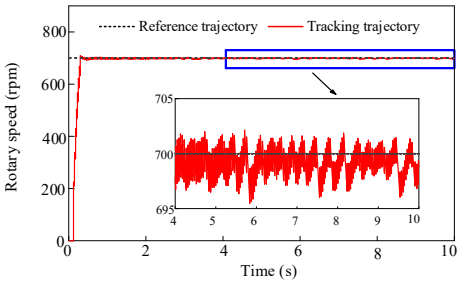

Fig. 13. Trajectory tracking results for 700 rpm rotary speed reference curve.

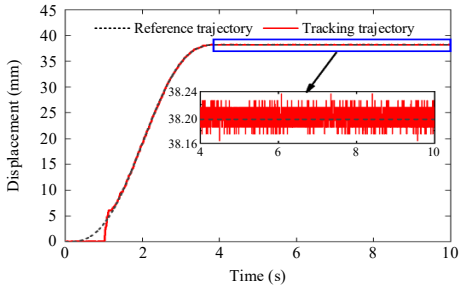

Fig. 14. Trajectory tracking results of ESO-SMC for step signal with smooth transition.

The proportional-integral-derivative (PID) control, with a long history, is the most common control approach used in practical applications. It has the advantages of simple structure, fast response speed, high stability and non-model-based, so the control strategy is suitable for pneumatic systems with strong nonlinearities. The experimental results of motion control with PID controller are shown in Figure 11(a), Figure 11(b) and Figure 12(a). The control parameters for the linear module are K_p=0.38, K_i=4.6, K_d=0.0128 , and the control parameters for the rotary module are K_p=0.25, K_i=0.22, K_d=0.004. It can be found from the experimental results that the PID controller achieves a maximum steady-state tracking error of 1.4 mm and a root mean square error of 0.441 mm in linear motion. In addition, the maximum steady state error achieved by the PID controller in rotary motion is about 15 rpm.

Accurate modeling of pneumatic actuators remains challenging due to nonlinear factors such as air compressibility and actuator friction. Linear active disturbance rejection control (LADRC) is widely used in pneumatic systems because it is characterized by low dependence on accurate mathematical modeling, high disturbance immunity, and fast response. The

experimental results of motion control using the LADRC controller are shown in Figure 11(c), Figure 11(d) and Figure 12(b). The control parameters for the linear module are λ_1=390, ω_0=31.5, b_0=5900, r=50000, h=0.001 and for the rotary module are λ_1=10, ω_0=15, b_0=500, r=5000, h=0.001. It is evident that the LADRC controller achieves a maximum steady-state tracking error and root mean square error of 0.8 mm and 0.398 mm, respectively, in linear motion. Furthermore, the maximum steady-state error in rotary motion is approximately 2.5 rpm. Compared to the PID controller, the LADRC controller demonstrates superior accuracy in controlling constant rotational speed.

The ESO-SMC controller designed in this paper is employed for motion control experiments and the results are shown in Figure 11(e), Figure 11(f) and Figure 12(c). In this regard, the control parameters of the linear module are λ_R=250, ω_0=25, Δ=0.1, b_0=3000, ε=1200, k=0.5, r=50000, h=0.001 and the control parameters of the rotary module are λ_R=250, ω_0=10, Δ=0.1, b_0=500, ε=200, k=0.5, r=5000, h=0.001. From the results of motion control experiments, it can be found that the maximum steady-state tracking error of 0.44 mm and the steady-state root mean square error of 0.176 mm can be realized with the LADRC controller. Moreover, the maximum steady-state error of the ESO-SMC controller is about 2 rpm. Obviously, ESO-SMC exhibits smaller maximum steady-state errors and root mean square errors compared to LADRC and PID. This demonstrates the effectiveness of the designed ESO-SMC controller, and ESO-SMC enables the linear-rotary composite motion pneumatic servo system to achieve high motion accuracy. The nonlinear robust controller in ESO-SMC has a good suppression effect on the system saturation phenomenon caused by the high gain of ESO, which can effectively improve the system steady-state control accuracy without affecting the system stability.

Figure 13 presents the tracking control performance of the ESO-SMC controller under a constant rotary speed reference of 700 rpm. Without adjusting the controller parameters, the ESO-SMC maintains control accuracy within a speed range of 696–702 rpm. The experimental results demonstrate that the proposed ESO-SMC controller exhibits strong robustness and achieves satisfactory speed tracking performance for the linear-rotary composite motion pneumatic actuator.

Finally, to analyze the positioning performance of the ESO-SMC controller, the reference signal is expressed as follows:

$$x_{ref}=\begin{cases}-(60/\pi^2)\sin(0.5\pi t)+30t/\pi, & t\le 4\\ -(60/\pi^2)\sin(0.5\pi t)+30t/\pi\big|_{t=4}, & t>4\end{cases} \tag{38}$$

The trajectory tracking results of the ESO-SMC controller are shown in Figure 14. It can be found that the trajectory tracking accuracy of the ESO-SMC controller is satisfactory, and its tracking error is within 0.04 mm. The experimental results show that ESO has a good estimation effect on the disturbances, and SMC has a significant suppression effect on the uncertainty and system instability caused by ESO. In general, for the developed linear-rotary composite motion pneumatic actuator, the ESO-SMC controller can achieve good tracking performance and positioning performance.

CONCLUSION AND OUTLOOK

This paper proposes a novel linear-rotary composite motion pneumatic actuator, which can achieve both linear motion and rotary motion. A linear-rotary composite motion servo system is further built for the pneumatic actuator using two proportional directional control valves. In addition, an extended state observer-based sliding mode control (ESO-SMC) algorithm is designed to realize high-precision position and speed control of the system. From the experimental results, it is found that:

1) In performing the linear motion of the pneumatic actuator, the ESO-SMC controller has a better tracking effect compared with the PID and LADRC controllers. The maximum steady-state error for tracking a sinusoidal reference signal with a 0.25 Hz frequency is 0.44 mm, and the steady-state positioning error is within 0.04 mm.

2) In performing the rotary motion of the actuator, ESO-SMC controller is able to realize faster adjustment time and better steady-state control accuracy. The maximum steady-state error for tracking an 800 rpm speed signal is approximately 2 rpm.

The above results demonstrate the feasibility of the proposed linear-rotary composite motion pneumatic actuator, with the ESO-SMC controller achieving significant control accuracy. In future research, we will explore advanced control algorithms to further improve position and speed tracking performance, with the goal of practical implementation. Additionally, we plan to develop a frictionless linear-rotary composite motion pneumatic actuator based on aerostatic gas lubrication principles to enhance efficiency and precision (Jia et al., 2024; Jia et al., 2025; Pu et al., 2025).

ACKNOWLEDGEMENTS

This work was supported by the National Natural Science Foundation of China (Grant No. 52575062), the Postgraduate Research and Practice Innovation Program of Jiangsu Province (Grant No. SJCX24_2404), and the Innovation and Practice Fund Project of the School of Artificial Intelligence and Intelligent Manufacturing of Jiangsu University (Grant No. ZXJG2023023).

REFERENCES

Ahmad F, Adeel M, Qiu B, et al. “Sowing uniformity of bed-type pneumatic maize planter at various seedbed preparation levels and machine travel speeds.” International Journal of Agricultural and Biological Engineering, 14(1): 165-171（2021）.

Bi Z, Luo C, Miao Z, et al. “Automatic robotic recharging systems–development and challenges.” Industrial Robot: the international journal of robotics research and application, 48(1): 95-109 (2021).

Chen S, Hung Y, Gong S. “Speed control of vane-type air motor servo system using proportional-integral-derivative-based fuzzy neural network.” International Journal of Fuzzy Systems, 18: 1065-1079(2016).

Chen S, Gong S. “Speed tracking control of pneumatic motor servo systems using observation-based adaptive dynamic sliding-mode control.” Mechanical Systems and Signal Processing, 94: 111-128(2017).

Gao H, De Volder M, Cheng T, et al. “A pneumatic actuator based on vibration friction reduction with bending/longitudinal vibration mode.” Sensors and Actuators A: Physical, 252: 112-119(2016).

Gu S, Yan C, Liu X, et al. “Prescribed performance control for a pneumatic cylinder with strong friction via nonlinear extended state observer.” International Journal of Hydromechatronics, 6(4): 359-379(2023).

Han L, Kumi F, Mao H, et al. “Design and tests of a multi-pin flexible seedling pick-up gripper for automatic transplanting.” Applied Engineering in Agriculture, 35(6):949-957(2019).

Huang M, Jiang X, He L, et al. “Development of a robotic harvesting mechanism for button mushrooms”. Transactions of the ASABE, 64(2): 565-575 (2021).

Jia Y, Zhang Z, Du S, et al. “Linear active disturbance rejection motion control of a novel pneumatic actuator with linear-rotary compound motion.” International Journal of Hydromechatronics, 7(4): 382-399 (2024).

Jia Y, Qian P, Zhang Z, et al. “Intelligent selection of parameters for air-floating piston based on improved multi-objective grey wolf optimisation algorithm.” International Journal of Hydromechatronics, 8(2): 121-147 (2025).

Liang Z, Xu L, De B, et al. “Optimisation of a multi-duct cleaning device for rice combine harvesters utilising CFD and experiments.” Biosystems Engineering, 190: 25-40(2020).

Liao C, Chen J, Geng F, et al. “Airflow basin structure numerical optimisation analysis and suction nozzle characteristics experimental study of vacuum-vibration tray precision seeder”. Journal of Agricultural Engineering, 53(4) (2022).

Liu J, Zhao S, Li N, et al. “Development and field test of an autonomous strawberry plug seeding transplanter for use in elevated cultivation.” Applied Engineering in Agriculture, 35(6): 1067-1078(2019).

Luo X, Wang J, Shpanin L, et al. “A new scroll-type air motor with magnetic spirals.” IEEE/ASME Transactions on Mechatronics, 23(1): 459-468(2018).

Ma G, Mao H, Han L, et al. “Reciprocating mechanism for whole row automatic seedling picking and dropping on a transplanter.” Applied Engineering in Agriculture, 36(5): 751-766(2020).

Mao H, Ma G, Han L, et al. “A whole row automatic pick-up device using air force to blow out vegetable plug seedlings.” Spanish Journal of Agricultural Research, 18(4): e0211-e0211 (2020).

Meng D, Tao G, Zhu X. “Adaptive robust motion trajectory tracking control of pneumatic cylinders.” Journal of Central South University, 20(12): 3445-3460(2013a).

Meng D, Tao G, Zhu X, et al. “Motion trajectory tracking control of pneumatic position servo systems.” Transactions of the Chinese Society for Agricultural Machinery, 44(4): 268-274(2013b).

Meng D, Tao G, Zhu X. “Integrated direct/indirect adaptive robust motion trajectory tracking control of pneumatic cylinders.” International Journal of Control, 86(9): 1620-1633(2013).

Pham T M, Twiefel J. “Ultrasonic friction reduction in elastomer-metal contacts and application to pneumatic actuators.” Physics Procedia, 70: 55-58(2015).

Pu C, Jia Y, Zhang Z, et al. “Intelligent optimization of air-floating piston core parameters for homemade frictionless pneumatic actuators based on a new multi-objective particle swarm optimization algorithm with Gaussian mutation and fuzzy logic.” Engineering Applications of Artificial Intelligence, 154: 111053 (2025).

Qian P, Ren X, Zhang L, et al. “Simultaneous control of motion and maximized stiffness for an electro-pneumatic clutch actuator based on pressure observers.” Advances in Mechanical Engineering, 9(6): 1-9(2017).

Qian P, Pu C, Liu L, et al. “A novel pneumatic actuator based on high-frequency longitudinal vibration friction reduction.” Sensors and Actuators A: Physical, 344: 113731(2022a).

Qian P, Pu C, He D, et al. “A method to improve the motion trajectory tracking accuracy of pneumatic servo system-by exciting longitudinal resonance.” Journal of the Brazilian Society of Mechanical Sciences and Engineering, 44: 376(2022b).

Qian P, Pu C, Liu L, et al. “Development of a new high-precision friction test platform and experimental study of friction characteristics for pneumatic cylinders.” Measurement Science and Technology, 33(6): 065001(2022c).

Qian P, Luo H, Liu L, et al. “A hybrid Gaussian

mutation PSO with search space reduction and its application to intelligent selection of piston seal grooves for homemade pneumatic cylinders." Engineering Applications of Artificial Intelligence, 122: 106156(2023a).

Qian P, Liu L, Pu C, et al. "Methods to improve motion servo control accuracy of pneumatic cylinders - review and prospect." International Journal of Hydromechatronics, 6(3): 274-310(2023b).

Qian P, Pu C, Liu L, et al. "A novel high-frequency resonance controllable pneumatic actuator and its high-precision motion trajectory tracking control." Mechatronics, 96: 103089(2023c).

Qian P, Liu L, Wu J, et al. "A novel double-acting, air-floating, frictionless pneumatic actuator." Sensors and Actuators A: Physical, 362: 114674(2023d).

Qian P, Pu C, Liu L, et al. "Ultra-high-precision pneumatic force servo system based on a novel improved particle swarm optimization algorithm integrating Gaussian mutation and fuzzy theory." ISA transactions, 152: 453-466 (2024a).

Qian P, Jia Y, Liu Lei, et al. "Nonlinear robust motion trajectory tracking control based on backstepping method for a novel pneumatic actuator." Journal of the Brazilian Society of Mechanical Sciences and Engineering, 46(7): 427(2024b).

Ren H, Huang C. "Adaptive backstepping control of pneumatic servo system." In: 2013 IEEE International Symposium on Industrial Electronics, pp. 1-6(2013).

Ren H, Fan J, Kaynak O. "Optimal design of a fractional-order proportional-integer-differential controller for a pneumatic position servo system." IEEE Transactions on Industrial Electronics, 66(8): 6220-6229(2019).

Saddam H, Hu J, Chen Y, et al. "CFD study of self-cleaning system of multi-stage tangential roller threshing unit for precise buckwheat breeding." Heliyon, 10(5): 2405-8440(2024).

Safak C, Topuz V, Fevzi Baba A. "Pneumatic motor speed control by trajectory tracking fuzzy logic controller." Sadhana, 35: 75-86(2010).

Soleymani F, Rezaei S M, Zareinejad M, et al. "Position control of a servo-pneumatic actuator with mis-matched uncertainty using multiple-surface sliding mode controller and high-gain observer." Transactions of the Institute of Measurement and Control, 39(10): 1497-1508(2017).

Sun G, Li S, Yu Q, et al. "Enhancing position control in pneumatic systems using ANFIS and high-speed on-off valves with compound PWM." International Journal of Hydromechatronics, 7(4): 347-367(2024).

Whitney J P, Glisson M F, Brockmeyer E L, et al. "A low-friction passive fluid transmission and fluid-tendon soft actuator." In: 2014 IEEE/RSJ International Conference on Intelligent Robots and Systems, pp. 2801-2808(2014).

Xie H, Zhang Z, Zhang K, et al. "Research on the visual location method for strawberry picking points under complex conditions based on composite models." Journal of the Science of Food and Agriculture, 104(14): 8566-8579 (2024).

Yue R, Hu J, Liu Y, et al. "Design and working parameter optimization of pneumatic reciprocating seedling-picking device of automatic transplanter." Agriculture, 12(12): 1989(2022).

Zhao L, Xia Y, Yang Y, et al. "Multicontroller positioning strategy for a pneumatic servo system via pressure feedback." IEEE Transactions on Industrial Electronics, 64(6): 4800-4809(2017).

Zhao L, Sun J, Yang H, et al. "Position control of a rodless cylinder in pneumatic servo with actuator saturation." ISA Transactions, 90: 235-243(2019).

Zhu Q, Zhang H, Zhu Z, et al. "Structural design and simulation of pneumatic conveying line for a paddy side-deep fertilisation system." Agriculture, 12(6): 867(2022).

Zong C, Li Q, Li K, et al. "Computational fluid dynamics analysis and extended adaptive hybrid functions model-based design optimization of an explosion-proof safety valve." Engineering Applications of Computational Fluid Mechanics, 16(1): 296-315 (2022).